Efficient 671 nm red light generation in annealed proton-exchanged periodically poled LiNbO₃ waveguides

Yunfei Niu (钮云飞), Lei Yang (杨 磊), Dongjie Guo (郭东洁), Yan Chen (陈 琰),
Xiaoyang Li (李晓阳), Gang Zhao (赵 刚)*, and Xiaopeng Hu (胡小鹏)**

National Laboratory of Solid State Microstructures, College of Engineering and Applied Sciences, and School of Physics,
Nanjing University, Nanjing 210093, China
*Corresponding author: zhaogang@nju.edu.cn; **corresponding author: xphu@nju.edu.cn

We report efficient generation of 671 nm red light based on quasi-phase-matched second harmonic generation of 1342 nm in LiNbO₃ waveguides. The design method and fabrication process of the high-quality annealed proton-exchanged periodically poled channel waveguides were presented. A continuous-wave 1.71 mW red light was obtained with a single-pass conversion efficiency of $47\% \cdot \mathrm{W}^{-1} \cdot \mathrm{cm}^{-2}$, which is 88% that of the theoretical value. While for 1 mW quasi-continuous-laser input, the corresponding peak power being 2 W, the conversion efficiency reached up to 60%. Our results indicate that the annealed proton-exchanged periodically poled LiNbO₃ waveguide is promising for high-efficiency and low power consumption nonlinear generation of visible light.

Keywords: lithium niobate; second-harmonic generation; optical waveguides; proton exchange.
doi: 10.3788/COL202018.111902.

Coherent red light sources at around 671 nm have important applications such as full-color laser display[1,2], optical cooling and trapping of lithium atoms[3], and generation of entangled beams in quantum information technology[4]. Frequency doubling of neodymium-doped solid-state lasers is a conventional approach to obtain 671 nm laser light sources, and nonlinear crystals based on the quasi-phase-matching technique are commonly used due to the high-frequency conversion efficiency. Generation of red light at 671 nm based on second-harmonic generation (SHG) using quasi-phase-matched bulk crystals has been demonstrated, such as single-pass SHG using periodically poled stoichiometric LiTaO₃[5,6] and extra-cavity frequency doubling with periodically poled KTiOPO₄[7]. Nonlinear interactions can be more efficient in waveguides compared with that in bulk crystals, because the light field is confined in a small cross section. In addition, high optical intensity is maintained over a long propagation length without divergence by diffraction, and thus efficient frequency conversions can be achieved in a single-pass configuration, reducing the complexity of the optical setup as compared to extra-cavity frequency conversions. There are several techniques to obtain the waveguide structure in LiNbO₃, such as annealed proton exchange (APE)[8], Ti indiffusion[9], and optical grade dicing[10,11]. APE LiNbO₃ waveguides show low propagation loss and fine nonlinear performance due to the annealing process. Besides, comparing with optical grade dicing, where the high-precision dicing technique is needed, the fabrication process of APE is relatively simple. High-performance quasi-phase-matched second-order nonlinear interactions have been demonstrated in APE periodically poled LiNbO₃ (PPLN) waveguides, such as generation of high-brightness

entangled photons[12], enhanced electro-optic spectral tuning device[13], and efficient third-harmonic generation in the communication band[14].

In this work, we designed and fabricated APE PPLN waveguides for 671 nm red light generation and characterized the SHG performances of the nonlinear waveguides. The normalized SHG efficiency was $47\% \cdot \mathrm{W}^{-1} \cdot \mathrm{cm}^{-2}$ for continuous-wave (CW) input at 1342 nm. In addition, when the quasi-continuous fundamental wave (FW) with a peak power of 2 W was used, the conversion efficiency was 60%.

To design the APE PPLN channel waveguides, the geometric structure and the poling period of the waveguide are the key parameters. Since the proton-exchange process only increases the extraordinary refractive index (n_e), only TM modes are supported in z-cut APE waveguides. The extraordinary refractive index change of the APE LiNbO₃ waveguide can be described as $\Delta n_e = \delta(\lambda) \cdot C(y, z)$, where $\delta(\lambda)$ is the wavelength-dependent coefficient, and $C(y, z)$ is the normalized proton concentration[15]. The profile of $C(y, z)$ is determined by the channel width W and the annealing depth D[16], and the annealing depths in the z direction and y direction were assumed to be the same for simplicity. To obtain low propagation loss, the surface proton concentration $C_0 \equiv C(0, 0)$ should be smaller than 0.23[16], and thus a relatively large annealing depth is required to support the guide mode in the near-infrared spectral range. The single-mode condition for the FW at 1342 nm was estimated as follows: $W = 6\,\mu\mathrm{m}$, $D = 3\,\mu\mathrm{m}$, and $0.12 < C_0 < 0.16$. The simulated refractive index increment of the TM₀₀ mode at 1342 nm and 671 nm is shown in Fig. 1(a). The effective refractive index of the TM₀₀ mode was numerically calculated using COMSOL
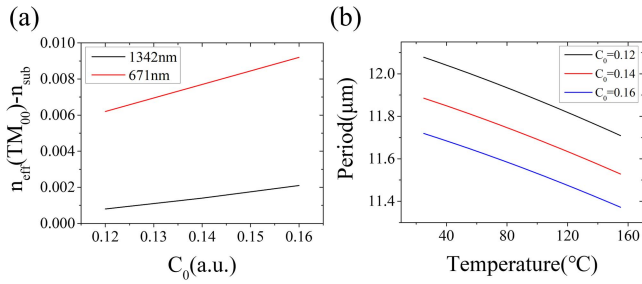
Fig. 1. (a) Refractive index increment as a function of surface proton concentration C_0 in 6 μm wide channel APE waveguides with annealing depth of 3 μm. (b) Theoretical poling period for our APE PPLN structure as a function of temperature, where the surface proton concentration C_0 varies from 0.12 to 0.16.

Fig. 2. (a) SEM picture of SiO_2 mask. (b) Image of the inverted domain structure of the APE waveguide recorded using confocal SH microscopy. (c) The measured and fitted transmission spectra of the waveguide.

Multiphysics, and the refractive index of the substrate was calculated based on the Sellmeier equation for the extraordinary index of congruent $LiNbO_3$[17]. When the surface proton concentration C_0 varied from 0.12 to 0.16, the refractive index increment of the FW changed from 0.0008 to 0.0021; while for the second-harmonic (SH) wave, the refractive index increment changed from 0.0062 to 0.0092. We chose three surface proton concentrations, C_0, 0.12, 0.14, and 0.16 and calculated the poling periods for the SHG processes varying with the working temperature, as shown in Fig. 1(b). The poling periods decrease slightly with increased temperature or increased surface proton concentration C_0. To reduce the photorefractive effect, the working temperature of the SHG process was set to be above 100°C, and thus the poling periods were designed to vary in the range from 11.30 to 12.02 μm, with intervals of 0.24 μm.

The detailed fabrication process for the channel APE PPLN waveguide is described as follows. Full-wafer periodical poling was obtained using the conventional electric field technique at room temperature[18]. Then a 200-nm-thick SiO_2 film was deposited on the PPLN wafer using plasma-enhanced chemical vapor deposition. Subsequent UV lithography and inductively coupled plasma etching were used to form the SiO_2 mask with open channels, and the channel waveguide structure was defined by the SiO_2 mask. For the APE $LiNbO_3$ channel waveguide, the waveguide pattern is defined by the SiO_2 mask, and thus the line edge roughness of the mask will transfer to the waveguide. To reduce the waveguide propagation loss caused by interface scattering[19], a fine-quality SiO_2 mask is required. From the scanning electron microscope (SEM) picture of the SiO_2 mask shown in Fig. 2(a), we can see that the edge of the etched groove shows fine quality, which ensures low propagation loss. The PPLN wafer was then diced into small chips with dimensions of 2.1 cm (L) × 1.0 cm (W) and proton exchanged in benzoic acid at 170°C for 3.5 h. The low temperature was chosen to keep low temperature sensitivity of the diffusion coefficient, thus reducing the impact of temperature fluctuations during the proton exchange[20]. Soft annealing at 210°C for 10 h was carried out to preserve the single crystalline
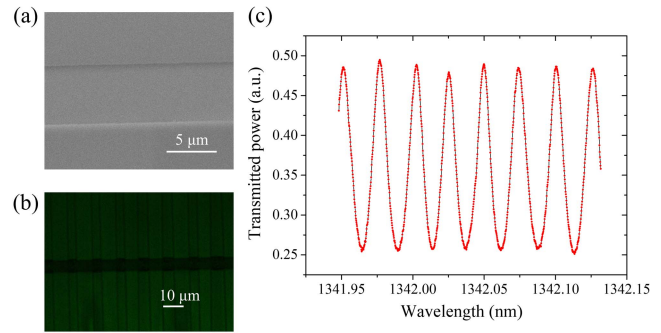
phase of the waveguides, which is helpful for reducing the propagation loss. Finally, the chips were annealed at 333°C for 15 h, and the diffusion depth was about 3 μm, with the waveguide width being 6 μm. Both facets of the chips were polished to facilitate end-fiber coupling. Using the confocal SH microscopy, the fabricated APE PPLN waveguide was characterized, as shown in Fig. 2(b). The duty cycle of the inverted domains was close to 50%, and the periodic domain structure was preserved after the APE process. The Fabry–Perot method[21] was used to measure the propagation loss of the channel waveguide with a CW fiber laser (Santech, TSL-550). Figure 2(c) shows the measured transmitted power when the wavelength of the input swept around 1342 nm at room temperature. By fitting the transmission curve, the propagation loss of the waveguide was calculated to be 0.097 dB/cm, which was attributed to the optimized proton-exchange process and the fine-quality SiO_2 mask. The low propagation loss in this work is at the same level as that in reversed proton-exchanged $LiNbO_3$ waveguides by Fejer's group[22], with the typical value being 0.1 dB/cm.

The schematic experimental setup for SHG of red light at 671 nm is shown in Fig. 3. The fundamental light source is a diode-pumped $Nd:YVO_4$ laser working at 1342 nm. The FW was gathered into a single-mode fiber and then coupled into the waveguide through a naked fiber. The fiber-to-chip coupling efficiency was measured to be ~35%, and the coupling efficiency would be higher by
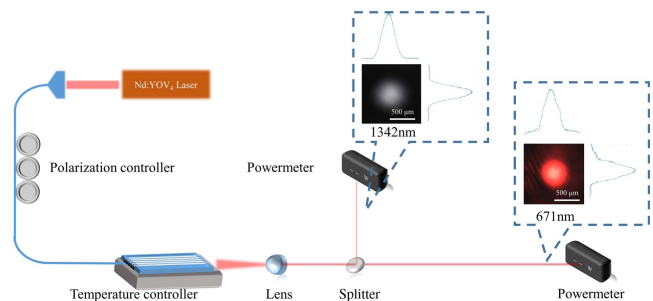

Fig. 3. Schematic experimental setup. The two insets are the images of the FW and SH wave, respectively.

choosing a lensed fiber, which can provide improved mode matching. A polarization controller was used to adjust the polarization of the FW to the vertical direction, which was required for excitation of the TM mode in the APE waveguide. The PPLN waveguide was embedded in an oven for temperature control. Light was coupled out from the waveguide by an aspherical mirror with a focal length of 10 mm. A beam splitter was used to separate the FW and SH waves for individual measurement. The spatial mode images of FW and SH waves recorded with CCD are shown in Fig. 3, and the intensity profiles in the vertical (depth) and horizontal (width) directions were presented as well. Both intensity profiles showed nearly Gaussian shape, which indicated that the interacting waves were in the TM_{00} mode in the waveguide.

Firstly, we turned off the Q-switch, the fundamental laser light source was in a CW operation mode, and we tested the single-pass SHG performance of the nonlinear waveguides at 1342 nm. SHG was achieved in the waveguides with poling periods of 11.78 and 12.02 μm, and the corresponding quasi-phase-matching temperature was measured to be 141.0°C and 40°C, respectively. According to the measured quasi-phase-matching temperature, the surface proton concentration was estimated to be 0.12, which was used to calculate the theoretical frequency conversion efficiency of the fabricated sample. We chose the waveguide with higher quasi-phase-matching temperature, and the temperature tuning curve of this waveguide is shown in Fig. 4. The temperature acceptance bandwidth of the waveguide was measured to be ~3.3°C, which was close to the theoretical value, as shown in Fig. 4. The output power of the SH wave at 141.0°C was 1.71 mW, and the corresponding power of the input FW was 28.7 mW. The normalized efficiency of SHG in quasi-phase-matched PPLN waveguides is given by[23]

$$\eta = \frac{8\pi^2}{\epsilon_0 c \lambda_{2\omega}^2} \frac{d_{\text{eff}}^2}{n_1^2 n_2} \frac{\iint E_{2\omega}^* E_w^2 \mathrm{d}x\mathrm{d}z}{\sqrt{\iint |E_{2\omega}|^2 \mathrm{d}x\mathrm{d}z \iint |E_\omega|^2 \mathrm{d}x\mathrm{d}z}}, \quad (1)$$

where n_1 and n_2 are the effective refractive indices of the waveguide modes at the FW and SH, respectively, ϵ_0 is the vacuum permittivity, and c is the speed of light in vacuum. The effective nonlinear coefficient $d_{\text{eff}} = 2d_{33}/\pi$ with $d_{33} = 20 \, \text{pm/V}$[24]. $E_\omega, E_{2\omega}$ are the electric fields of the 1342 nm TM_{00} and 671 nm TM_{00} modes, respectively. Thus, the theoretical normalized SHG efficiency was calculated to be $53\% \cdot W^{-1} \cdot cm^{-2}$. The normalized SHG efficiency was measured to be $47\% \cdot W^{-1} \cdot cm^{-2}$, which was ~88% of the theoretical value. $LiNbO_3$ is a good electro-optic material[25,26], and it is possible to tune the SHG conversion efficiency of the APE PPLN waveguide by integrated electrodes. What one should note is that the duty cycle of the periodically poled structure should deviate from 0.5 when the electrical field is applied along the z direction of the $LiNbO_3$ crystal[13].

The SHG conversion efficiency as a function of the input power of the FW is shown in Fig. 5(a). The conversion efficiency is proportional to the power of the input FW, and a maximum conversion efficiency of 11.5% was obtained when the power of the FW reached 70 mW. The stability of the output over time at the maximum output was tested. The power fluctuation was less than 10% for the first 20 min. After 1 h, the output power decreased gradually to 60% that of the maximum output. The maximum output can be recovered when we turned off the input FW for dozens of minutes. The reduction of efficiency is due to the phase mismatch caused by the photorefractive effect. To characterize the waveguide performance at high input powers, we switched the near-infrared laser to the Q-switched operation mode, and the laser delivered pulsed output with 50 ns pulse duration and 10 kHz repetition rate. The SHG conversion efficiency varies with the average power of the pulsed FW, as shown in Fig. 5(b), which shows a linear relationship. When the average power of FW was 1 mW, the corresponding peak power being 2 W, the conversion efficiency of SHG reached up to 60%.

To conclude, we have designed and fabricated periodically poled channel APE $LiNbO_3$ waveguides for efficient 671 nm red light generation. The channel
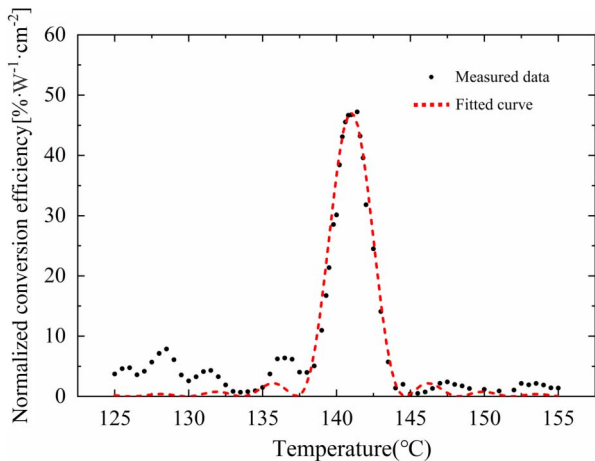
Fig. 4. Temperature tuning curve of APE PPLN waveguide with 11.78 μm poling period. The black dots and the dashed red line are the measured data and fitted curve, respectively.
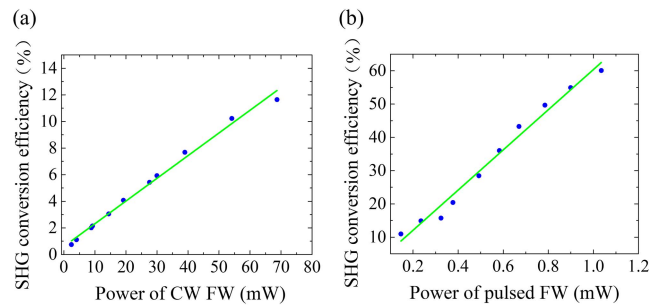
Fig. 5. Measured SHG conversion efficiency as a function of the power of FW with (a) CW and (b) 50 ns, 10 kHz pulsed input. The blue dots and the green line correspond to the measured conversion efficiency and the linear fitting curve, respectively.

waveguides were fabricated on PPLN by the APE technique. By optimizing the fabrication process, the PPLN channel waveguides with 0.097 dB/cm low propagation loss were obtained, and the waveguide exhibited excellent SHG performance. With CW input, 1.71 mW red light was obtained with normalized efficiency up to $47\% \cdot \mathrm{W}^{-1} \cdot \mathrm{cm}^{-2}$, which is nearly 90% that of the theoretical value. The SHG conversion efficiency reached up to 60% when pulsed FW with an average power of 1 mW was coupled into the waveguide. Our work provides a scheme for high-efficiency red light generation. To further raise the power-handle capacity of the APE periodically poled waveguide, MgO-doped LiNbO$_3$ can be used as the host material[27,28], which possesses higher photorefractive damage threshold.

References

1. M. S. Brennesholtz, in *SID Symposium Digest of Technical Papers* (2008), paper 39.1:858-861.
2. Y. X. Zhang, Y. L. Yang, L. H. Zhang, D. Z. Lu, M. Xu, Y. Hang, S. S. Yan, H. H. Yu, and H. J. Zhang, Chin. Opt. Lett. **17**, 071402 (2019).
3. M. S. Safronova, U. I. Safronova, and C. W. Clark, Phys. Rev. A **86**, 042505 (2012).
4. J. H. Kimble, Nature **453**, 1023 (2008).
5. X. P. Hu, X. Wang, Z. Yan, H. X. Li, J. L. He, and S. N. Zhu, Appl. Phys. B Lasers Opt. **86**, 265 (2007).
6. X. P. Hu, P. Xu, and S. N. Zhu, Photon. Res. **1**, 171 (2013).
7. X. Cui, Q. Shen, M. Yan, C. Zeng, T. Yuan, W. Zhang, X. Yao, C. Peng, X. Jiang, Y. Chen, and J. Pan, in *Conference on Lasers and Electro-Optics* (2019), paper JTu2A.92.
8. R. Roussev, X. P. Xie, K. Parameswaran, and M. M. Fejer, in *16th Annual Meeting of the IEEE Lasers and Electro-Optics Society* (2003), p. 338.
9. J. Li, Y. Yao, J. Wu, and Z. Qi, in *International Photonics and Optoelectronics Meetings* (2012), paper IF4A.11.
10. N. Kretzschmar, U. Eismann, F. Sievers, F. Chevy, and C. Salomon, Opt. Express **25**, 14840 (2017).
11. N. Courjal, B. Guichardaz, G. Ulliac, J. Y. Rauch, B. Sadani, H. H. Lu, and M. P. Bernal, J. Phys. D. Appl. Phys. **44**, 305101 (2011).
12. H. Jin, F. M. Liu, P. Xu, J. L. Xia, M. L. Zhong, Y. Yuan, J. W. Zhou, Y. X. Gong, W. Wang, and S. N. Zhu, Phys. Rev. Lett. **113**, 103601 (2014).
13. Y. Y. Lin, Y. F. Chiang, Y. C. Huang, A. C. Chiang, S. T. Lin, and Y. H. Chen, Opt. Lett. **31**, 3483 (2006).
14. M. Marangoni, M. Lobino, and R. Ramponi, Opt. Lett. **31**, 2707 (2006).
15. R. V. Roussev, "Optical-frequency mixers in periodically poled lithium niobate: materials, modeling and characterization," PhD. Thesis (Stanford University, 2006).
16. G. B. Hocker and W. K. Burns, Appl. Opt. **16**, 113 (1977).
17. D. H. Jundt, Opt. Lett. **22**, 1553 (1997).
18. S. N. Zhu, Y. Y. Zhu, Z. Y. Zhang, H. Shu, H. F. Wang, J. F. Hong, C. Z. Ge, and N. B. Ming, J. Appl. Phys. **77**, 5481 (1995).
19. A. Boudrioua, *Photonic Waveguides: Theory and Applications* (Wiley, 2009).
20. F. Lenzini, S. Kasture, B. Haylock, and M. Lobino, Opt. Express **23**, 1748 (2015).
21. S. Taebi, M. Khorasaninejad, and S. S. Saini, Appl. Opt. **47**, 6625 (2008).
22. R. V. Roussev, C. Langrock, J. R. Kurz, and M. M. Fejer, Opt. Lett. **29**, 1518 (2004).
23. J. Y. Chen, Y. M. Sua, Z. H. Ma, C. Tang, Z. Li, and Y. P. Huang, OSA Continuum **2**, 2914 (2019).
24. I. Shoji, T. Kondo, A. Kitamoto, M. Shirane, and R. Ito, J. Opt. Soc. Am. B **14**, 2268 (1997).
25. Y. Yang, X. Deng, H. Lao, and X. F. Chen, Chin. Opt. Lett. **9**, 021901 (2011).
26. Q. Y. Li, J. Huo, X. H. Zhao, and X. F. Chen, Chin. Opt. Lett. **12**, 050701 (2014).
27. H. Y. Liu, Y. J. Yu, D. H. Sun, H. Liu, Y. H. Wang, H. Zheng, D. Li, and G. Y. Jin, Chin. Opt. Lett. **17**, 111404 (2019).
28. B. Bai, Y. Bai, D. Li, Y. X. Sun, J. L. Li, and J. T. Bai, Chin. Opt. Lett. **16**, 031402 (2018).